OPTICA

Ultrafast 550-W average-power thin-disk laser oscillator

Moritz Seidel,* Lukas Lang, Christopher R. Phillips,† and Ursula Keller†

Institute for Quantum Electronics, Department of Physics, ETH Zurich, 8093 Zurich, Switzerland
†*These authors contributed equally to this work.*
**seidelm@phys.ethz.ch*

Received 3 May 2024; revised 22 August 2024; accepted 22 August 2024; published 23 September 2024

SESAM modelocked oscillators are interesting for applications in strong-field physics such as high-harmonic generation and attosecond science at high repetition rates or frequency combs in the ultraviolet. Here we present a SESAM modelocked ultrafast thin-disk laser oscillator providing 550 W of average output power with 852 fs pulses at 5.5 MHz repetition rate. To reach this significant power scaling, a replicating cavity design for modelocked oscillators is utilized. The oscillator delivers 103 MW of peak power with a pulse energy of 100 μJ at a beam quality of $M^2 < 1.2$, with a high optical-to-optical efficiency of 35%. The advances in SESAM design and manufacturing that enabled this result are discussed, as well as practical challenges when scaling oscillators to the kW-class. When combined with established pulse compression technologies, this oscillator can enable simpler systems by avoiding the complexity of chirped pulse amplifier chains. Additionally, high power oscillators support a much lower noise floor due to the reduced influence of shot noise, which may provide a route to more sensitive pump-probe measurements.

https://doi.org/10.1364/OPTICA.529185

1. INTRODUCTION

High-average-power laser sources find many applications in research and industry, both in continuous-wave (cw) and ultrafast operation. While these are often realized in MOPA (master oscillator power amplifier) configurations with thin-disk, slab, or fiber gain geometries [1–3], a compelling alternative strategy is to power scale the laser oscillator itself. The thin-disk laser geometry [4] uses disks with a thickness of typically around 100 μm operated in reflection. This architecture offers extremely efficient heat removal along the axis of the disk, as well as ultra-low optical nonlinearities since the laser beam only propagates through a small amount of material. Consequently, thin-disk technology has emerged as the most suitable one for oscillator power scaling, with output powers of up to 4 kW demonstrated in fundamental mode cw operation [5]. There has been an extensive research effort to develop high-power ultrafast oscillators using thin-disk technology [6,7] to drive nonlinear processes without the complexity of chirped-pulse amplifier (CPA) chains.

In the context of attosecond science [8], there has been a major effort to scale high-harmonic-generation (HHG) systems to high pulse repetition rates [9–11]: such scaling can speed up certain measurements by orders of magnitude, and in some configurations gives access to frequency comb spectroscopy in the extreme ultraviolet [12]. High-power Yb-based laser systems have been a critical part of these efforts, for example, enabling HHG powers at the milliwatt level using fiber CPA systems [13]. Thin-disk oscillators offer a potentially simpler solution by driving high-repetition-rate HHG directly with an oscillator [14–16]. Since Yb lasers have lower bandwidths than traditional Ti:sapphire lasers, nonlinear compression is often needed to reach the best HHG performance. Fortunately, nonlinear compression in multipass cells (MPCs) has become an established and power-scalable approach [17,18], including in the few-cycle regime relevant for isolated attosecond pulse generation at MHz repetition rates [19]. Thin-disk oscillators are excellent candidates for driving MPC compression setups [20–22] since they provide clean and transform-limited soliton pulses at high repetition rates with excellent beam quality. In addition to attosecond science, thin-disk oscillators have also been successfully deployed for driving powerful terahertz sources [23–25] and high-power optical parametric oscillators [26].

Modelocking of a thin-disk laser (TDL) was first obtained by incorporating a SESAM into the cavity [27], and operating the laser in the soliton modelocking regime [28]. SESAM modelocked TDLs typically have an optimal operating point of several hundred femtoseconds due to the competing effects of spatial hole burning in the thin-disk and the moderate gain bandwidth of the gain medium (e.g., Yb:YAG) [29]. Quite early on in their development, it was observed that excessive self-phase modulation (SPM) in the intracavity air could prevent soliton modelocking [30]. This SPM issue was avoided by operation inside an evacuated or helium-filled environment [30,31]. Later, it was shown that the vacuum chamber can be avoided by using cascaded quadratic nonlinearities to add an equal and opposite amount of SPM, resulting in a 210 W laser operated in air [32]. Another important theme in TDL systems has been the deployment of active multipass cells [33–36], which allow operation at large output coupling rates and therefore

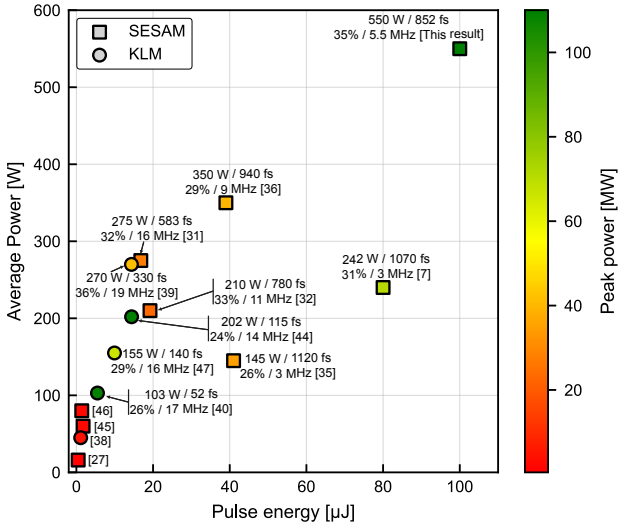

Fig. 1. Overview of semiconductor saturable absorber mirror (SESAM) and Kerr lens modelocked (KLM) thin-disk laser oscillators using Yb-doped gain media. The color of the data points corresponds to the achieved peak power of the oscillator output. Some are marked with average output power, pulse duration, optical-to-optical efficiency, and repetition rate. Results are selected if they exceed 100 W average output power or if they presented power records at time of their publication. The corresponding references are [7,27,31,32,35,36,38–40,44–47].

allow scaling to higher average output powers and pulse energies while placing less stringent demands on the intracavity optics. While early work focused on SESAM modelocking, later work revealed the viability of alternative modelocking regimes such as with the frequency-doubling nonlinear mirror [37] and Kerr-lens modelocking (KLM) [38].

To date the two techniques offering the highest average power have been KLM (with up to 270 W [39]) and SESAM modelocking (with up to 350 W [36]). Comparing these two approaches, SESAM modelocking supports more robust cavity design strategies while KLM supports significantly shorter pulses. A particularly notable example of this was the recent demonstration of a 52 fs oscillator with 103 W average power [40]. This approach is very promising for directly driving efficient HHG sources without compression [41]. On the other hand, MPC compression is now mature and offers an efficient route to obtain few-cycle pulses starting from the ∼800 fs pulses usually delivered by SESAM-modelocked TDLs, typically achieved by cascading multiple MPC compression stages [42,43].

Here, we present a new milestone in scaling of ultrafast oscillators with a record breaking 550-W average power thin-disk oscillator. This laser also provides the highest pulse energy of any ultrafast oscillator, 100 μJ, surpassing the long-standing previous record of 80 μJ [7]. Furthermore, the laser provides 852-fs-long pulses at 5.5 MHz repetition rate resulting in a peak power of 103 MW, which is the highest peak power of any SESAM modelocked oscillator to date. All of this is achieved at a high optical-to-optical efficiency of 35%. Figure 1 gives an overview of published high-power and high-energy modelocked thin-disk laser oscillators.

This result is made possible by combining several advancements in thin-disk laser architecture: First, the use of a multipass cavity design without a focus inside the multipass scheme, optimized through an improved understanding of the influence of aberrations on cavity mode [48]. This leads to a smaller Gouy phase of the cavity when compared with other multipass architectures. Second, the use of more compact, water-cooled mirror mounts; and finally, advancements in SESAM design and bonding the SESAM to sapphire [49].

2. EXPERIMENTAL SETUP

The setup schematic is shown in Fig. 2(a). The gain medium is a 100-μm-thick Yb-doped disk with a cold radius of curvature of −3.84 m bonded onto a diamond heat sink (TRUMPF Scientific Lasers). The disk is used in a 44-pass module and pumped into the 940 nm absorption band. The pump spot on the disk (full width at half maximum of the flat top beam) is adjusted to a radius of 3.7 mm, while the cavity is designed such that the single mode laser spot size on the disk is 2.7 mm ($1/e^2$ radius). The corresponding spot size ratio is 73%, which lies within the usual 70%–80% range that has been confirmed experimentally and numerically [48] to yield good performance. Using GTI-type dispersive mirrors, a nominal −57200 fs^2 of round-trip group-delay dispersion (GDD) is introduced. To avoid cavity mode deterioration caused by thermal effects on these mirrors, at most −2000 fs^2 GDD per single mirror is used. These highly negative GDD mirrors are predominantly placed in positions with large mode size such that the fluence on them stays comparatively small to avoid damage [7].

Figure 2(b) shows the laser mode radius evolution along the cavity axis, including six reflections on the thin-disk (12 reflections per round-trip) via the replicating cavity active multipass arrangement. The lengths of a single segment [shaded green in Fig. 2(b)] of the cavity are as follows: from output coupler to convex mirror 1500 mm, from convex mirror to thin-disk 1230 mm, and from thin-disk to folding point 1290 mm. This is then replicated in reverse order as seen in Fig. 2(b) until six passes are achieved. The convex mirrors have a radius of curvature of 2000 mm. In the telescope towards the SESAM [shaded orange in Fig. 2(b)], concave mirrors with −1000 mm and −2000 mm radius of curvature are used.

This multipass design was proposed for oscillators in 2016 [50,51] but only shown as a proof concept and not demonstrated for high-power operation. This paper is the first time this cavity design is used for high-power or modelocked oscillator operation. In thin-disk amplifiers similar multipass designs are also used [1,52–54].

Here, a 40% output coupler was used. With four passes on the disk (eight reflections per round-trip), we achieved 420 W of output power using a 30% output coupler [55].

The cavity mode radius evolution shows that only one tight focus is present inside the cavity, which helps limit the amount of SPM picked up in the gas environment. By integrating the intensity of the Gaussian beam through each free space segment in the cavity, it is straightforward to show that the round-trip B-integral is proportional to the round-trip Gouy phase. The new cavity design yields a round-trip Gouy phase of 5.7π (resulting in an estimated round-trip B-integral of 133 mrad at 550 W produced by the residual air, the thin-disk itself, and the sapphire on top of the SESAM), whereas the $4f$ cavity design used in the last record-power result had a significantly higher Gouy phase of 9.6π [36].

During simulation of this cavity, it is important to consider the soft aperture effect of the thin-disk via an additional imaginary

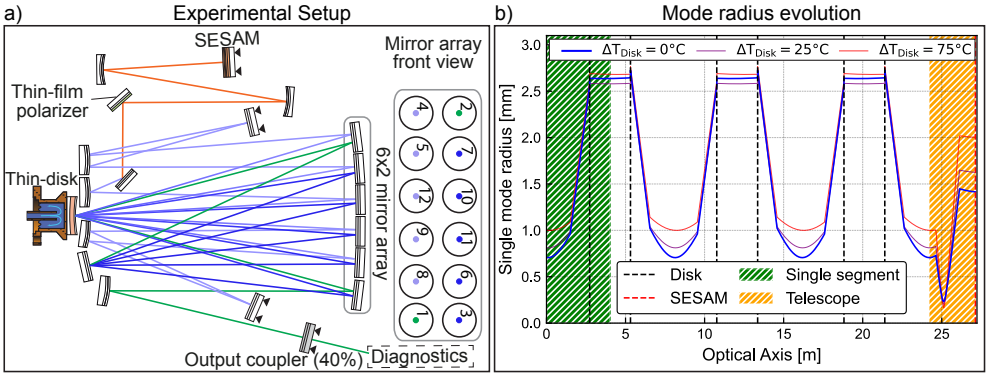

Fig. 2. Laser cavity design. The beam path is shown in (a), where the shade of blue indicates the height above the optical table of the beam. The mirrors in the mirror array are numbered in sequence of hits if traced starting from the output coupler. For simplicity, not all flat folding mirrors are shown. Almost all mirrors are negatively dispersive with values of -550 fs^2, -1200 fs^2, -1300 fs^2, or -2000 fs^2 of group delay dispersion (GDD). Some mirrors (symbolized with two triangles on their backside in the schematic) are motorized with piezo actuators for automatic alignment of the laser passes onto the disk. The first segment as well as the telescope to the SESAM are color coded green and orange, respectively, corresponding to the shaded color in (b) where the laser mode radius evolution throughout the cavity is shown. Three different power points parametrized by the change in disk temperature are shown. The nominal cold cavity mode is shown in blue, with cavity mode simulations for hotter disks depicted in purple and red.

radius of curvature of the thin-disk to correct for length-mismatch-induced breakup of the cavity stability zone [50]. This cavity design has a wide stability range where the laser spot size falls within 70% − 80% of the pump spot size. In fact, with this design, the stability range is independent of the number of passes on the disk, which is in stark contrast to previously used 4 f-imaging-like designs [35,36] and thus has the same stability zone as a simple convex-concave cavity. In principle, this fact allows arbitrary scaling of the number of passes on the disk without affecting the stability zone, which was previously not possible.

To reduce the misalignment, the mirrors in the array are mounted on a custom machined baseplate which ensures minimal segment-to-segment length misalignment, which is extremely crucial for this cavity design.

Furthermore, as can be seen from Fig. 2(b), the cavity is stable over a wide range of disk temperatures, which relates to values of the thermal lens of the disk as presented in [48]. The cavity was also designed such that for increasing temperature of the disk (and thus increased thermal lensing), the mode size on the SESAM increases. This helps reduce the fluence of the SESAM for larger powers and increases the range of stable modelocking.

3. SESAM DESIGN AND MANUFACTURING

In its simplest form, a SESAM consists of a distributed Bragg reflector (DBR) with a quantum well region on top [56]. Typical solid-state lasers achieving watt-level output powers utilize one to three quantum wells and target spot sizes on the SESAM on the order of 100 μm. While the same principles are used for high-power SESAMs, the combination of high average power and high pulse energy places stringent demands on the device, and imposes additional physical and technical constraints that arise with power scaling. To address these challenges, we have developed a new type of SESAM that is based on ion implantation of a multi-quantum well structure combined with a semiconductor top-coating that is silicate bonded to a sapphire superstrate. Figure 3 shows the production process and SESAM layer structure as well as the bonding quality obtained for this result. In the rest of this section, we describe the key aspects of the new SESAM.

A. Thin-Film Structure

For the use in high-power lasers a relatively high saturation fluence F_{sat} and high rollover fluence F_2 are critical. It is now standard practice to apply a top-coating (TC) to the quantum well (QW) region of the SESAM in order to reduce the electric field in the quantum wells and thereby increase the saturation fluence [57]. Since the product $F_{sat}\Delta R$ scales with the number of quantum wells, devices that use a TC to obtain high F_{sat} also require multiple QW layers to achieve a reasonable ΔR [57]. Designs with as many as six QWs have been explored for high-power SESAMs [58], but this required distributing the QW layers between multiple antinodes of the electric field with strain compensation in between. Therefore, here we have chosen a simpler and thinner structure with three QWs in a single anti-node.

SESAM TC structures based on dielectric materials or semiconductor materials have been explored [57]. While semiconductor TCs offer simplicity since they can be incorporated into the same epitaxial growth run as the QW, dielectric TC's have the advantage of lower nonlinearities and higher damage threshold compared to semiconductor layers. Therefore, dielectric TCs became the technique of choice for high-power SESAMs. However, another consideration involved in the choice of TC is the capability of bonding the SESAM to a superstrate. In earlier work we showed that silicate bonding is a useful approach for high-power SESAMs with an athermal or even inverted thermal response [49]. So far, our implementation of the silicate bonding process requires a semiconductor TC instead of the dielectric TC. Therefore, here we use a semiconductor TC design. As can be seen in Fig. 3(b), the TC reduces the electric field enhancement inside the QWs to about 0.28 at 1030 nm (compared to a theoretical value of 0.51 without top-coating).

B. Sample Growth and Bonding

Another consideration with power scaling is achieving high surface quality over a large area, which is a well-known challenge with SESAMs. The InGaAs QW layers are normally grown at low temperature (LT) to introduce mid-gap traps [59,60] that result in an ultrafast recovery, but this approach tends to exhibit reduced

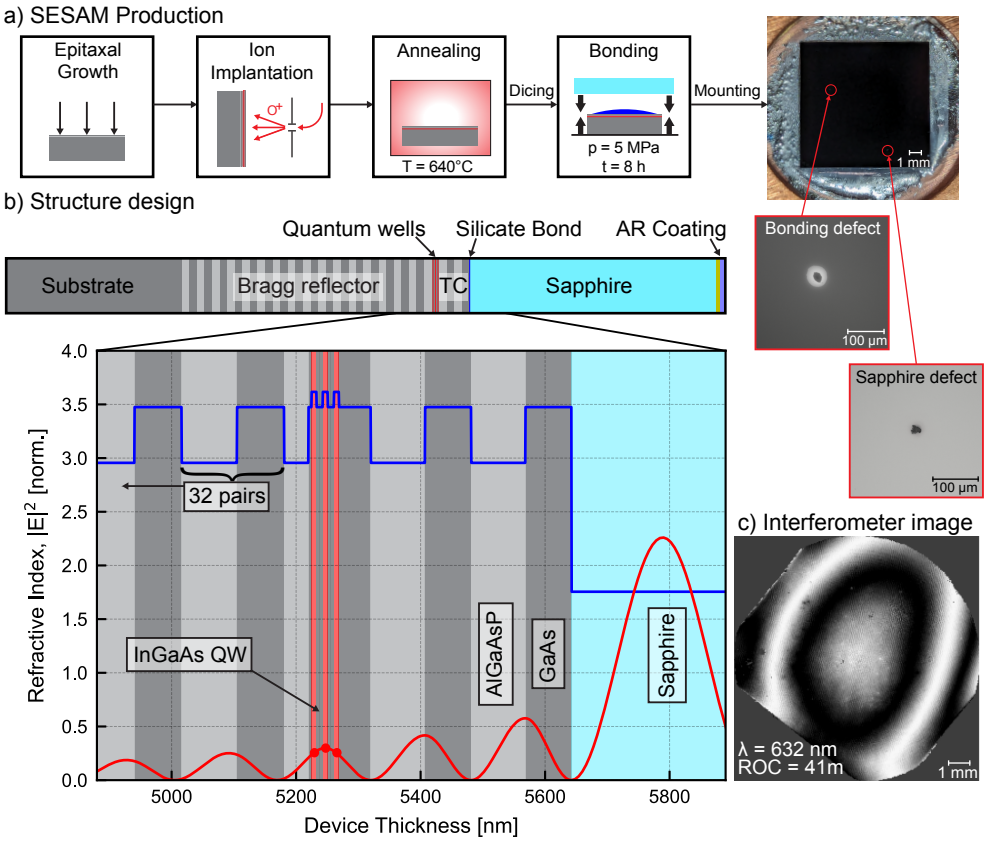

Fig. 3. SESAM used for this result. (a) Schematic steps of the production process with macro pictures of the bonded SESAM showing the 10 mm × 10 mm bonding interface and zoom in to two defects in the otherwise flawless bond. (b) Layer structure for the designed SESAM with a zoom in on top region of the grown structure. GaAs (dark gray), AlGaAsP (light gray, 2% gallium and 1% phosphorus), InGaAs quantum wells (light red, indium content optimized for absorption edge at 1060 nm), and the bonded sapphire (light blue) are shown. The refractive index is shown in solid blue and the calculated standing electric field in red at 1030 nm (normalized to four outside the structure and sapphire). (c) Interferometer image of the bonded and mounted SESAM with an average residual radius of curvature (ROC) of 41 m (measured at 632 nm through the sapphire).

surface quality as well as significant variations in the recovery time between different growth runs. Therefore, we have revisited the ion implantation approach [61,62]: instead of using LT growth, the sample is grown with MOVPE under optimal high-temperature conditions and traps are introduced in the QWs by a post-growth ion implantation step to obtain a picosecond recovery time. Specifically, to ensure the surface is free of defects we grow the DBR and TC layers with strain-compensation by introducing 1% of phosphorus into the AlGaAsP regions. The quantum wells are thin enough to not require strain compensation themselves. We choose high-temperature growth for both the DBRs and the quantum wells to achieve low defect density in all layers.

Subsequently, oxygen ion implantation of the quantum wells is performed to intentionally induce defects for a tailored and reduced recovery time. Here, an induced defect density of $1.2 \times 10^{19}/\mathrm{cm}^3$ is targeted inside the quantum wells. For high growth quality, the quantum wells are placed in a pure GaAs region. The samples are also annealed at 640°C after ion implantation, which influences the non-saturable losses and recovery time [63]. The growth, ion implantation, and annealing were performed at Ferdinand-Braun-Institut (FBH) in Berlin.

Square samples are diced from the wafer and silicate bonded to a 1-mm-thick wedged sapphire window [49]. We observe that this results in an improved cold curvature of the SESAM, while simultaneously giving a more desirable thermal lensing behavior. The semiconductor is cleaved into $10 \times 10\ \mathrm{mm}^2$ samples as this is five times the expected largest beam diameter on the SESAM in the experiment (Fig. 2). We have made some adaptations to the bonding process described initially in [49], mainly now applying a constant pressure of 5 MPa to the silicate bond for 8 h while curing. This increases the bond quality and longevity of the samples noticeably, possibly due to a thinner bond interface. The utilized sapphires are a-cut to mitigate the effects of any stress-induced depolarization effects and are mounted in the laser in such a way that the polarization axis aligns with the polarization selected by the thin-film polarizer (TFP) inside the cavity.

After bonding, the SESAMs have a radius of curvature in the range of 40 m as can be seen in Fig. 3(c). This residual radius of curvature is still on the order of the cavity length and should not be neglected. If the deformation is assumed to be purely parabolic, a residual radius of curvature on this order can be compensated for by translating the SESAM very slightly along the cavity axis by a few millimeters. It is therefore straightforward to account for the SESAM curvature in the cavity design, which has a single mode spot radius targeted on the SESAM in the range of 1.5–2.0 mm as can be seen in Fig. 2(b).

The bonded, ion-implanted SESAM is characterized using a wide dynamic range nonlinear reflectivity setup with a measurement concept as described in [64]. The measurement is performed at a central wavelength of 1030 nm and a pulse duration

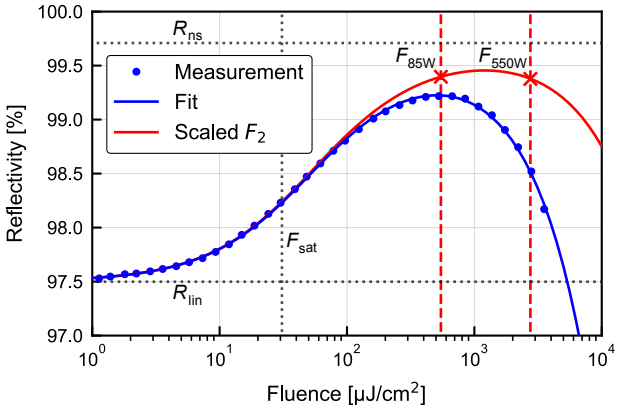

Fig. 4. Nonlinear reflectivity measurement of the SESAM used. The fit to the raw data (blue), as well as the reflectivity curve when scaling the inverse saturable absorbance parameter F_2 as described in the text are shown (red). The linear reflectivity R_{lin}, non-saturable reflectivity R_{ns}, and saturation fluence F_{sat} are shown with dotted lines. The fluences reached at the modelocking starting point at 85 W ($F_{85\,\mathrm{W}}$) and the operating point at 550 W ($F_{550\,\mathrm{W}}$) are indicated as red vertically dashed lines and marked with crosses on the scaled curve.

of 195 fs. This yields a saturation fluence of $F_{\mathrm{sat}} = 30.9\ \mu\mathrm{J/cm^2}$, an inverse saturable absorbance parameter of $F_2 = 243\ \mathrm{mJ/cm^2}$, a modulation depth of $\Delta R = 2.21\%$, and a non-saturable loss of $\Delta R_{\mathrm{ns}} = 0.29\%$. It should be noted that this value for ΔR_{ns} also already includes the residual losses of the anti-reflection coating of the sapphire, and is comparable to values obtained from traditional non-ion-implanted SESAMs. The complete nonlinear reflectivity curve is shown in Fig. 4. To correctly interpret this measurement of the SESAM for use in the thin-disk laser, the inverse saturable absorption parameter F_2 needs to be scaled with the pulse lengths of the thin-disk laser and the saturation measurement laser ($\tau_{\mathrm{TDL}}/\tau_{\mathrm{Fsat}} = 852$ fs/195 fs) [65,66].

The ultrafast response of the SESAM is characterized using a collinear dual-comb pump-probe measurement (similar to [67]) at 1030 nm. The measurement uses 700-fs-long pulses, and yielded a SESAM recovery time of 4.2 ps. In the context of the bi-exponential behavior of SESAM recovery typically observed when performing pump-probe measurements with 100 fs pulses [67], the 4.2 ps recovery time is the "slow" time scale.

As can be seen from the excellent optical-to-optical efficiency of the laser, the ion implantation, even when done through the relatively thick semiconductor top coating, does not impact the efficiency of the laser negatively. In fact, up to 380 W output power, the modelocked configuration yields more than 97% of the power of the cw configuration without a SESAM. This underscores the effectiveness of the new growth and processing avenue for achieving specifically tailored recovery times that hold up even against the most extreme conditions present in a high-power oscillator.

4. TECHNICAL CAVITY DESIGN CONSIDERATIONS

Most optics are mounted in custom in-house manufactured flexure mirror mounts. These mounts allow for optimal low-distortion mirror mounting. This is achieved by using a wavespring to apply three-point mounting pressure on the mirror surface in combination with water cooling of the individual mounts. The array of the 12 mirrors placed in front of the disk is also custom machined and water cooled, and ensures precise mounting positions and angles to reduce length differences between subsequent passes, which has been shown to be very critical in simulation [51].

Still, even with water-cooling and mounting on a low-distortion breadboard, due to vacuum being pulled inside the chamber and slow thermal drifts, some in-situ alignment is necessary to keep the output power stable. For this some cavity mirrors are motorized with piezo motors for automatic alignment [highlighted in Fig. 2(a)]. This provides enough degrees of freedom such that all passes on the disk can be moved. By optimizing the output power, the six reflections of the disk are all moved to the middle of the pump spot for optimal overlap, which is monitored by imaging the fluorescence of the pump spot. The automatic optimization does not disturb modelocking and is able to stabilize slow drifts very reliably.

It should be noted that special cavity design considerations must be made for high-power cavities. The thin-disk can only handle the high incident pump power ($> 3\ \mathrm{kW/cm^2}$) during lasing operation and is possibly damaged if lasing suddenly stops due to issues such as fast alignment drift, damage on other cavity components, or mechanically blocking the cavity. As a fail-safe, a second out-of-plane V-shaped multimode cavity in single pass configuration with a 19% output coupler is built. This cavity has a significantly higher lasing threshold than the main cavity, but can take over lasing instantly if the main cavity turns off.

During regular modelocked operation the pulse energy in the cavity is constrained by soliton formation and therefore stays within the damage threshold of all the intracavity optics. However, while optimizing these lasers it is possible to reach sub-optimal intermediate configurations where Q-switching instabilities are not suppressed well enough, leading to giant pulses in the cavity. By default, such events damage the SESAM as it is usually the lowest damage threshold optic in the cavity. To protect against this, a 'sacrificial' negative GDD mirror ($-550\ \mathrm{fs^2}$) is intentionally placed directly into the only tight focus inside the cavity (spot size radius 150 μm) which will experience much higher fluences than the SESAM. In case unexpected Q-switching occurs, the damage threshold of the sacrificial mirror in the focus is reached and the mirror damaged before the SESAM is catastrophically damaged.

5. MODELOCKING RESULTS

As mentioned above, the oscillator is operated in a vacuum chamber. We can finely control the pressure of the residual air to control the amount of self-phase modulation inside the oscillator. This helps us to obtain modelocked operation of the oscillator over a wide power range, from 85 W up to 550 W as can be seen in Fig. 5(a). Initial modelocking at 85 W is performed at atmospheric pressure and started by inducing some perturbation by tapping the vacuum chamber. At the highest power the residual air pressure is 33 mbar, with additional contributions to self-phase modulation coming mainly from the disk itself, the sapphire bonded onto the SESAM, and to a lesser extent the cavity optics themselves [7]. Due to this, the pulse length can consistently stay around 700 fs − 1000 fs, which is the optimal operating point for such an oscillator due to spatial hole burning in the Yb:doped gain medium used [29].

Figures 5(c)–5(f) show the modelocking diagnostics at 550 W of average output power. The pulses are almost transform limited

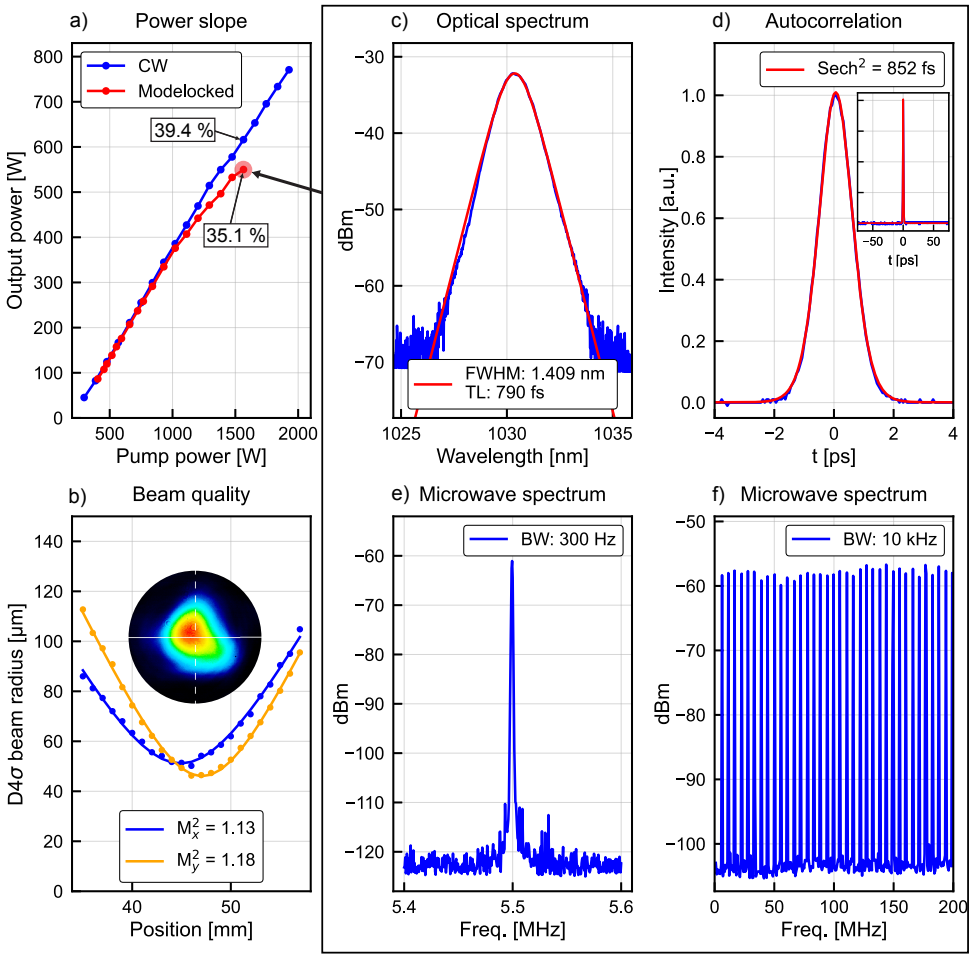

Fig. 5. Output diagnostics of the oscillator. (a) Power slope for the continuous-wave (blue) and modelocked (red) case with the optical-to-optical efficiency indicated for select data points. (b) Beam quality measurement and beam profile in the far field at the highest output power of 550 W. (c) Optical spectrum indicating a FWHM of 1.409 nm and transform limit (TL) of 790 fs. (d) Autocorrelation spectrum indicating a pulse length of 852 fs, with an inset showing a long-time window without satellite pulses. (e) Microwave spectrum indicating a repetition rate of 5.5 MHz and showing clean modelocking without sidebands around the repetition rate with 300 Hz resolution bandwidth. (f) Microwave spectrum spanning up to 200 MHz showing up to the 36th harmonic of the repetition rate with 10 kHz resolution bandwidth. All measurements shown in (b)–(f) were performed at 550 W average output power.

with the pulse length reaching 1.08 times the theoretical value of the optical limit. This is well in line with past results for high-power thin-disk laser oscillators. Both the optical spectrum and the autocorrelation spectrum do not show any artifacts and indicate clean modelocking. The autocorrelation trace is scanned over the whole autocorrelation range (200 ps) to make sure that no satellite pulses are present. The output beam quality was measured with a commercial M^2 measuring system (Thorlabs BP109-IR, compliant with ISO 11146) as shown in Fig. 5(b). At 550 W of output power the beam quality factor is $M^2 = 1.13 \times 1.18$ in the horizontal and vertical axes, respectively. With these values, the oscillator provides a better output beam quality than reported by recent thin-disk amplifier results [1,53]. The optical-to-optical efficiency of this oscillator during modelocked operation at 550 W output power is 35.1%. At the same pump power, in cw operation without SESAM (but with the TFP and all highly dispersive mirrors installed) the laser reaches 39.4% optical-to-optical efficiency. The intensity noise of the oscillator was not characterized.

The output power of the oscillator is currently limited by the fluence incident on the SESAM (2750 µJ/cm^2), which already operates it inside the rollover regime, as well as the onset of thermal distortions leading to mode degradation. To achieve even higher output powers, a larger SESAM would need to be bonded to be able to increase the spot size and thus decrease the fluence on the SESAM as well as the cavity adapted to better compensate for the thermal distortions, with both changes being non-trivial.

6. CONCLUSION

We present an ultrafast thin-disk laser oscillator providing 550 W of average power with 852-fs-long pulses at 5.5 MHz repetition rate resulting in a pulse energy and peak power of 100 µJ and 103 MW, respectively. This is, to the best of our knowledge, the highest average power and highest pulse energy ever achieved for any modelocked oscillator. Thus, this oscillator sets a new benchmark for high-power modelocking performance and shows the competitiveness of oscillators when compared with amplifier systems.

This result was enabled by the new replicating cavity design that allows for scaling the number of passes on the thin-disk without shrinking the cavity stability zone, which has been a roadblock for scaling the average power of ultrafast oscillators before.

Additionally, significant improvements in high-power SESAM technology, especially the use of high-temperature-grown quantum wells with subsequent ion implantation for careful recovery time control and further development of the silicate bonding technique, were instrumental in achieving the presented result.

The output parameters of this oscillators make it very interesting for applications in strong-field physics such as high-harmonic generation and attosecond science at high repetition rates, especially when combined with established multipass-cell pulse compression technology. Furthermore, such an oscillator is well suited for industrial applications such as micromachining of metals, glasses, and semiconductors where high average powers and pulse lengths on the order of 1 ps are often desired.

Funding. Schweizerischer Nationalfonds zur Förderung der Wissenschaftlichen Forschung (200020_200416).

Acknowledgment. We would like to thank Dr. Moritz Brendel and Prof. Dr. Markus Weyers from Ferdinand-Braun-Institut (FBH) Berlin for growth and ion implantation of the SESAM wafer used for this work. We would like to thank Marcel Baer from the engineering bureau at D-PHYS for designing the custom mirror mounts used and the mechanical workshop at D-PHYS for manufacturing them. We thank Dr. Valentin Wittwer for providing some of the highly dispersive mirrors used in this work. We thank TRUMPF Scientific Lasers for providing the thin-disk module and head.

Disclosures. The authors signed an NDA with TRUMPF with regards to the thin-disk module and head.

Data availability. Data underlying the figures presented in this paper is available at the ETH Zurich Research Collection library. Additional data may be obtained from the authors upon reasonable request.

REFERENCES

1. T. Dietz, M. Jenne, D. Bauer, *et al.*, "Ultrafast thin-disk multi-pass amplifier system providing 1.9 kW of average output power and pulse energies in the 10 mJ range at 1 ps of pulse duration for glass-cleaving applications," Opt. Express **28**, 11415–11423 (2020).
2. P. Russbueldt, T. Mans, J. Weitenberg, *et al.*, "Compact diode-pumped 1.1 kW Yb: YAG Innoslab femtosecond amplifier," Opt. Lett. **35**, 4169–4171 (2010).
3. M. Müller, C. Aleshire, A. Klenke, *et al.*, "10.4 kW coherently combined ultrafast fiber laser," Opt. Lett. **45**, 3083–3086 (2020).
4. A. Giesen, H. Hügel, A. Voss, *et al.*, "Scalable concept for diode-pumped high-power solid-state lasers," Appl. Phys. B **58**, 365–372 (1994).
5. S. Nagel, B. Metzger, T. Gottwald, *et al.*, "Thin disk laser operating in fundamental mode up to a power of 4 kW," in *The European Conference on Lasers and Electro-Optics* (Optical Society of America 2019), pp. 4–5.
6. J. Drs, J. Fischer, N. Modsching, *et al.*, "A decade of sub-100-fs thin-disk laser oscillators," Laser Photonics Rev. **17**, 2200258 (2023).
7. C. J. Saraceno, F. Emaury, C. Schriber, *et al.*, "Toward millijoule-level high-power ultrafast thin-disk oscillators," IEEE J. Sel. Top. Quantum Electron. **21**, 106–123 (2015).
8. P. Agostini, F. Krausz, and A. L'Huillier, "Nobel Prize in Physics 2023, for experimental methods that generate attosecond pulses of light for the study of electron dynamics in matter," (2023).
9. C. M. Heyl, J. Güdde, A. L'Huillier, *et al.*, "High-order harmonic generation with μJ laser pulses at high repetition rates," J. Phys. B **45**, 074020 (2012).
10. R. Klas, A. Kirsche, M. Gebhardt, *et al.*, "Ultra-short-pulse high-average-power megahertz-repetition-rate coherent extreme-ultraviolet light source," PhotoniX **2**, 4 (2021).
11. T. Witting, M. Osolodkov, F. Schell, *et al.*, "Generation and characterization of isolated attosecond pulses at 100 kHz repetition rate," Optica **9**, 145–151 (2022).
12. I. Pupeza, C. Zhang, M. Högner, *et al.*, "Extreme-ultraviolet frequency combs for precision metrology and attosecond science," Nat. Photonics **15**, 175–186 (2021).
13. S. Hädrich, J. Rothhardt, M. Krebs, *et al.*, "Single-pass high harmonic generation at high repetition rate and photon flux," J. Phys. B **49**, 172002 (2016).
14. F. Labaye, M. Gaponenko, V. J. Wittwer, *et al.*, "Extreme ultraviolet light source at a megahertz repetition rate based on high-harmonic generation inside a mode-locked thin-disk laser oscillator," Opt. Lett. **42**, 5170–5173 (2017).
15. F. Emaury, A. Diebold, C. J. Saraceno, *et al.*, "Compact extreme ultraviolet source at megahertz pulse repetition rate with a low-noise ultrafast thin-disk laser oscillator," Optica **2**, 980–984 (2015).
16. J. Fischer, J. Drs, F. Labaye, *et al.*, "Intra-oscillator high harmonic generation in a thin-disk laser operating in the 100-fs regime," Opt. Express **29**, 5833–5839 (2021).
17. J. Schulte, T. Sartorius, J. Weitenberg, *et al.*, "Nonlinear pulse compression in a multi-pass cell," Opt. Lett. **41**, 4511–4514 (2016).
18. A.-L. Viotti, M. Seidel, E. Escoto, *et al.*, "Multi-pass cells for post-compression of ultrashort laser pulses," Optica **9**, 197–216 (2022).
19. F. J. Furch, T. Witting, M. Osolodkov, *et al.*, "High power, high repetition rate laser-based sources for attosecond science," J. Phys.: Photonics **4**, 032001 (2022).
20. C.-L. Tsai, F. Meyer, A. Omar, *et al.*, "Efficient nonlinear compression of a mode-locked thin-disk oscillator to 27 fs at 98 W average power," Opt. Lett. **44**, 4115–4118 (2019).
21. G. Barbiero, H. Wang, M. Graßl, *et al.*, "Efficient nonlinear compression of a thin-disk oscillator to 8.5 fs at 55 W average power," Opt. Lett. **46**, 5304–5307 (2021).
22. S. Goncharov, K. Fritsch, and O. Pronin, "Amplification-free GW-level, 150 W, 14 MHz, and 8 fs thin-disk laser based on compression in multipass cells," Opt. Lett. **49**, 2717–2720 (2024).
23. C. J. Saraceno, "Mode-locked thin-disk lasers and their potential application for high-power terahertz generation," J. Opt. **20**, 044010 (2018).
24. Y. Wang, T. Vogel, M. Khalili, *et al.*, "High-power intracavity single-cycle THz pulse generation using thin lithium niobate," Optica **10**, 1719–1722 (2023).
25. F. Meyer, N. Hekmat, T. Vogel, *et al.*, "Milliwatt-class broadband THz source driven by a 112 W, sub-100 fs thin-disk laser," Opt. Express **27**, 30340–30349 (2019).
26. L. Lang, C. P. Bauer, C. R. Phillips, *et al.*, "51-W average power, 169-fs pulses from an ultrafast non-collinear optical parametric oscillator," Opt. Express **29**, 36321–36327 (2021).
27. J. Aus der Au, G. J. Spühler, T. Südmeyer, *et al.*, "16.2-W average power from a diode-pumped femtosecond Yb:YAG thin disk laser," Opt. Lett. **25**, 859–861 (2000).
28. F. X. Kartner, I. D. Jung, and U. Keller, "Soliton mode-locking with saturable absorbers," IEEE J. Sel. Top. Quantum Electron. **2**, 540–556 (1996).
29. R. Paschotta, J. Aus der Au, G. J. Spühler, *et al.*, "Passive mode locking of thin-disk lasers: effects of spatial hole burning," Appl. Phys. B **72**, 267–278 (2001).
30. S. V. Marchese, T. Südmeyer, M. Golling, *et al.*, "Pulse energy scaling to 5 μJ from a femtosecond thin disk laser," Opt. Lett. **31**, 2728–2730 (2006).
31. C. J. Saraceno, F. Emaury, O. H. Heckl, *et al.*, "275 W average output power from a femtosecond thin disk oscillator operated in a vacuum environment," Opt. Express **20**, 23535–23541 (2012).
32. F. Saltarelli, A. Diebold, I. J. Graumann, *et al.*, "Self-phase modulation cancellation in a high-power ultrafast thin-disk laser oscillator," Optica **5**, 1603–1606 (2018).
33. J. Neuhaus, J. Kleinbauer, A. Killi, *et al.*, "Passively mode-locked Yb:YAG thin-disk laser with pulse energies exceeding 13 μJ by use of an active multipass geometry," Opt. Lett. **33**, 726–728 (2008).
34. J. Neuhaus, D. Bauer, J. Zhang, *et al.*, "Subpicosecond thin-disk laser oscillator with pulse energies of up to 25.9 microjoules by use of an active multipass geometry," Opt. Express **16**, 20530–20539 (2008).
35. D. Bauer, I. Zawischa, D. H. Sutter, *et al.*, "Mode-locked Yb:YAG thin-disk oscillator with 41 μJ pulse energy at 145 W average infrared power and high power frequency conversion," Opt. Express **20**, 9698–9704 (2012).
36. F. Saltarelli, I. J. Graumann, L. Lang, *et al.*, "Power scaling of ultrafast oscillators: 350-W average-power sub-picosecond thin-disk laser," Opt. Express **27**, 31465–31474 (2019).
37. F. Saltarelli, A. Diebold, I. J. Graumann, *et al.*, "Modelocking of a thin-disk laser with the frequency-doubling nonlinear-mirror technique," Opt. Express **25**, 23254–23266 (2017).
38. O. Pronin, J. Brons, C. Grasse, *et al.*, "High-power 200 fs Kerr-lens mode-locked Yb:YAG thin-disk oscillator," Opt. Lett. **36**, 4746–4748 (2011).

39. J. Brons, V. Pervak, E. Fedulova, *et al.*, "Energy scaling of Kerr-lens mode-locked thin-disk oscillators," Opt. Lett. **39**, 6442–6445 (2014).
40. J. Fischer, J. Drs, N. Modsching, *et al.*, "Efficient 100-MW, 100-W, 50-fs-class Yb:YAG thin-disk laser oscillator," Opt. Express **29**, 42075–42081 (2021).
41. J. Drs, F. Trawi, M. Müller, *et al.*, "Intra-oscillator high harmonic source reaching 100-eV photon energy," Opt. Express **32**, 17424–17432 (2024).
42. A.-L. Viotti, C. Li, G. Arisholm, *et al.*, "Few-cycle pulse generation by double-stage hybrid multi-pass multi-plate nonlinear pulse compression," Opt. Lett. **48**, 984–987 (2023).
43. P. Balla, A. Bin Wahid, I. Sytcevich, *et al.*, "Postcompression of picosecond pulses into the few-cycle regime," Opt. Lett. **45**, 2572–2575 (2020).
44. S. Goncharov, K. Fritsch, and O. Pronin, "110 MW thin-disk oscillator," Opt. Express **31**, 25970–25977 (2023).
45. E. Innerhofer, T. Südmeyer, F. Brunner, *et al.*, "60-W average power in 810-fs pulses from a thin-disk Yb:YAG laser," Opt. Lett. **28**, 367–369 (2003).
46. F. Brunner, E. Innerhofer, S. V. Marchese, *et al.*, "Powerful red-green-blue laser source pumped with a mode-locked thin disk laser," Opt. Lett. **29**, 1921–1923 (2004).
47. J. Brons, V. Pervak, D. Bauer, *et al.*, "Powerful 100-fs-scale Kerr-lens mode-locked thin-disk oscillator," Opt. Lett. **41**, 3567–3570 (2016).
48. M. Seidel, L. Lang, C. R. Phillips, *et al.*, "Influence of disk aberrations on high-power thin-disk laser cavities," Opt. Express **30**, 39691–39705 (2022).
49. L. Lang, F. Saltarelli, G. Lacaille, *et al.*, "Silicate bonding of sapphire to SESAMs: adjustable thermal lensing for high-power lasers," Opt. Express **29**, 18059–18069 (2021).
50. K. Schuhmann, K. Kirch, and A. Antognini, "Multi-pass oscillator layout for high-energy mode-locked thin-disk lasers," arXiv, (2016).
51. K. Schuhmann, "The thin-disk laser for the 2S-2 P measurement in muonic helium," Ph.D. thesis (ETH Zurich, 2017).
52. M. Zeyen, L. Affolter, M. Abdou Ahmed, *et al.*, "Compact 20-pass thin-disk multipass amplifier stable against thermal lensing effects and delivering 330 mJ pulses with M2<1.17," Opt. Express **32**, 1218–1230 (2024).
53. M. Abdou Ahmed, C. Roecker, A. Loescher, *et al.*, "High-power ultrafast thin-disk multipass amplifiers for efficient laser-based manufacturing," Adv. Opt. Technol. **10**, 285–295 (2021).
54. J.-P. Negel, A. Voss, M. A. Ahmed, *et al.*, "1.1 kW average output power from a thin-disk multipass amplifier for ultrashort laser pulses," Opt. Lett. **38**, 5442–5445 (2013).
55. M. Seidel, L. Lang, C. R. Phillips, *et al.*, "Modelocked thin-disk laser oscillator providing more than 400 W average output power with a replicating cavity design," in *Laser Congress (ASSL, LAC)* (Optica Publishing Group, 2023), paper ATu4A.7.
56. U. Keller, "Ultrafast lasers," in *Graduate Texts in Physics* (Springer International Publishing, 2021).
57. C. J. Saraceno, C. Schriber, M. Mangold, *et al.*, "SESAMs for high-power oscillators: design guidelines and damage thresholds," IEEE J. Sel. Top. Quantum Electron. **18**, 29–41 (2012).
58. A. Diebold, T. Zengerle, C. G. E. Alfieri, *et al.*, "Optimized SESAMs for kilowatt-level ultrafast lasers," Opt. Express **24**, 10512–10526 (2016).
59. X. Liu, A. Prasad, J. Nishio, *et al.*, "Native point defects in low-temperature-grown GaAs," Appl. Phys. Lett. **67**, 279–281 (1995).
60. U. Siegner, R. Fluck, G. Zhang, *et al.*, "Ultrafast high-intensity nonlinear absorption dynamics in low-temperature grown gallium arsenide," Appl. Phys. Lett. **69**, 2566–2568 (1996).
61. M. J. Lederer, B. Luther-Davies, H. H. Tan, *et al.*, "Nonlinear optical absorption and temporal response of arsenic- and oxygen-implanted GaAs," Appl. Phys. Lett. **74**, 1993–1995 (1999).
62. M. J. Lederer, V. Kolev, B. Luther-Davies, *et al.*, "Ion-implanted InGaAs single quantum well semiconductor saturable absorber mirrors for passive mode-locking," J. Phys. D **34**, 2455 (2001).
63. H. H. Tan, C. Jagadish, M. J. Lederer, *et al.*, "Role of implantation-induced defects on the response time of semiconductor saturable absorbers," Appl. Phys. Lett. **75**, 1437–1439 (1999).
64. D. J. H. C. Maas, B. Rudin, A. R. Bellancourt, *et al.*, "High precision optical characterization of semiconductor saturable absorber mirrors," Opt. Express **16**, 7571–7579 (2008).
65. M. Haiml, R. Grange, and U. Keller, "Optical characterization of semiconductor saturable absorbers," Appl. Phys. B **79**, 331–339 (2004).
66. R. Grange, M. Haiml, R. Paschotta, *et al.*, "New regime of inverse saturable absorption for self-stabilizing passively mode-locked lasers," Appl. Phys. B **80**, 151–158 (2005).
67. A. Nussbaum-Lapping, C. R. Phillips, B. Willenberg, *et al.*, "Absolute SESAM characterization via polarization-resolved non-collinear equivalent time sampling," Appl. Phys. B **128**, 24 (2022).